

# Katsevich-Type Algorithms for Variable Radius Spiral Cone-Beam CT

Hengyong Yu

College of Communication Engineering, Hangzhou Dianzi University  
Hangzhou, Zhejiang 310018, China  
[yuhengyong@hotmail.com](mailto:yuhengyong@hotmail.com)

Yangbo Ye

Department of Mathematics, University of Iowa  
Iowa City, Iowa 52242, USA,  
[Yangbo-ye@uiowa.edu](mailto:Yangbo-ye@uiowa.edu)

Ge Wang

Department of Radiology, University of Iowa  
Iowa City, Iowa 52242, USA  
[ge-wang@uiowa.edu](mailto:ge-wang@uiowa.edu)

## ABSTRACT

To solve the long object problem, an exact and efficient algorithm has been recently developed by Katsevich. While the Katsevich algorithm only works with standard helical cone-beam scanning, there is an important need for nonstandard spiral cone-beam scanning. Specifically, we need a scanning spiral of variable radius for our newly proposed electron-beam CT/micro-CT prototype. In this paper, for variable radius spiral cone-beam CT we construct two Katsevich-type cone-beam reconstruction algorithms in the filtered backprojection (FBP) and backprojected filtration (BPF) formats, respectively. The FBP algorithm is developed based on the standard Katsevich algorithm, and consists of four steps: data differentiation, PI-line determination, slant filtration and weighted backprojection. The BPF algorithm is designed based on the scheme by Zou and Pan, and also consists four steps: data differentiation, PI-line determination, weighted backprojection and inverse Hilbert transform. Numerical experiments are conducted with mathematical phantoms

Keywords: Computed tomography (CT), Katsevich algorithm, spiral cone-beam scanning, filtered backprojection (FBP), backprojected filtration(BPF)

## 1. INTRODUCTION

To solve the long object problem in the field of computed tomography (CT), a first level of improvement was made by performing 3D-backprojection of 1D-filtered cone-beam data collected along a spiral/spiral-like locus. The prototype of this approach is the algorithm by Wang *et al.*<sup>1</sup>. Over the past decade, numerous reconstruction algorithms were designed to improve the reconstruction quality<sup>2-8</sup>. Wang *et al.* categorized these algorithms into three categories: exact, approximate and iterative algorithms<sup>9</sup>. The exact algorithms would reconstruct accurate images if projection data are completely and noiseless. The approximate algorithms could outperform the exact algorithms when data are incomplete, noisy or involved with moving objects. The iterative algorithms are preferred when data are very noisy or incomplete. However, none of these earlier algorithms are both theoretically exact and computationally efficient to handle longitudinally truncated cone-beam data collected from a spiral locus.

To address the above problem, Katsevich recently proposed an exact and efficient algorithm<sup>10-13</sup>, which is a significant breakthrough in the area of spiral cone-beam CT. The Katsevich algorithm is in a filtered backprojection format and formulated in terms of the so-called PI-line and Tam-Danielsson window in the case of the standard helical scanning. The algorithm relies on that any point inside the scanning helix belongs to one and only one PI-line. Because it does not require data from multiple spiral turns, which are needed by other exact algorithms, the Katsevich algorithm is much more efficient and allows much better temporal resolution than earlier

exact algorithms, while it also eliminates image artifacts associated with approximate algorithms. As a result, it has attracted increasing interests<sup>14-21</sup>.

While the Katsevich algorithm only works with standard helical cone-beam scanning, there is an important need for nonstandard spiral cone-beam scanning. Specifically, we need a scanning spiral of variable radius for our newly proposed electron-beam CT/micro-CT<sup>22</sup> prototype to facilitate dynamic volumetric imaging. In our EBCT/EBMCT design, an electron beam is electromagnetically steered to produce cone-beam projections continuously on a detector surface enclosing a patient/animal. For that purpose, we generalized the Tam-Danielsson detection window and studied the existence and uniqueness of the PI-line in the case of variable radius spiral cone-beam scanning<sup>18</sup>. We proved that any point in a certain region inside a nonstandard 3D spiral would be passed by one and only one PI-line if the curvature of the corresponding planar spiral could always remain positive. Also, we implemented the Katsevich algorithm<sup>15</sup> in planar detector geometry. In this paper, we will mainly study Katsevich-type cone-beam reconstruction with a nonstandard spiral locus. Here we use Katsevich-type reconstruction to cover 3D methods with spiral cone-beam projection data based on the PI-line and Tam-Danielsson window.

This paper is organized as follows. The next section defines systems and notations. Section III describes two Katsevich-type algorithms, FBP and BPF, for variable radius spiral cone-beam scanning. Different from the Katsevich algorithm, Zou and Pan proposed another exact image reconstruction algorithm by changing the order of backprojection and filtration of cone-beam data derivatives<sup>16</sup>. Hence, in addition to the Katsevich-type FBP algorithm based on Katsevich's generic formulation, we also have the Katsevich-type BPF algorithm based on the work by Zou and Pan. Section IV evaluates our nonstandard spiral cone-beam reconstruction algorithms in numerical simulation. Finally, section V concludes the paper.

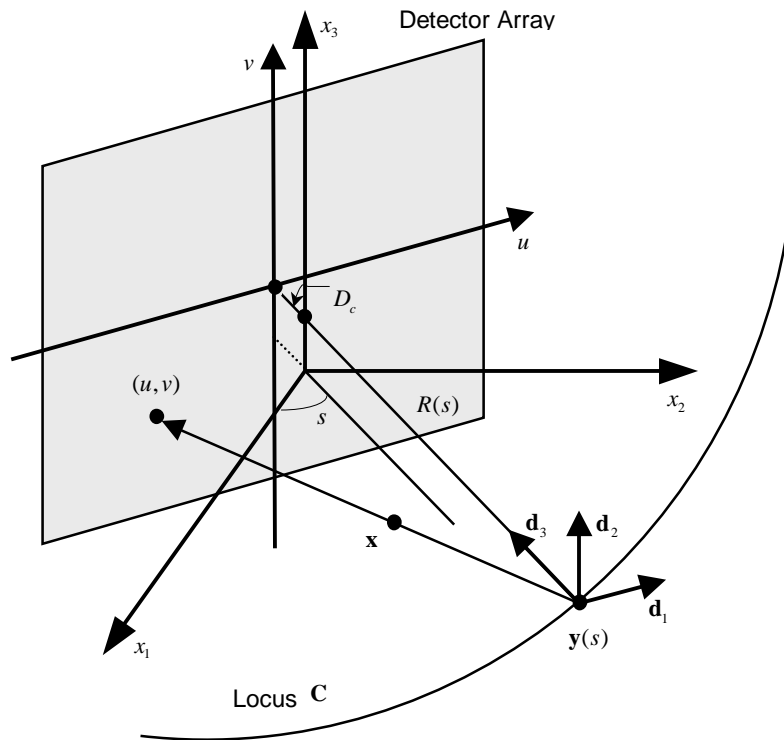


Figure 1. Local coordinate system for cone-beam projection measurement on a planar detector.

## 2. SYSTEMS AND NOTATIONS

Consider an object function  $f(\mathbf{x})$  whose support is a cylindrical region  $\mathbf{U}$ . For any unit vector  $\boldsymbol{\beta}$ , let us define the cone-beam projection of  $f(\mathbf{x})$  from a source position  $\mathbf{y}(s)$  by

$$D_f(\mathbf{y}(s), \boldsymbol{\beta}) = \int_0^{\infty} f(\mathbf{y}(s) + t\boldsymbol{\beta}) dt. \quad (1)$$

For our electron-beam CT/micro-CT configuration, we describe a variable radius spiral locus as

$$\mathbf{C} := \left\{ \mathbf{y}(s) \in \mathbb{R}^3 : y_1 = R(s) \cos(s), y_2 = R(s) \sin(s), y_3 = \frac{sh}{2\pi}, s \in \mathbb{R} \right\} \quad (2)$$

For a given  $s$ , we define a local coordinate system by its three orthogonal unit directional vectors:  $\mathbf{d}_1 := (-\sin(s), \cos(s), 0)$ ,  $\mathbf{d}_2 := (0, 0, 1)$  and  $\mathbf{d}_3 := (-\cos(s), -\sin(s), 0)$ . Shown as in Fig. 1, cone-beam data are measured on a planar detector array parallel to  $\mathbf{d}_1$  and  $\mathbf{d}_2$  at a distance  $D(s)$  from  $\mathbf{y}(s)$  with  $D(s) = R(s) + D_c$ , where  $D_c$  is a constant. A detector position in the array is given by a pair of values  $(u, v)$ , which are signed distances along  $\mathbf{d}_1$  and  $\mathbf{d}_2$  respectively. Let  $(u, v) = (0, 0)$  correspond to the orthogonal projection of  $\mathbf{y}(s)$  onto the detector array. If  $s$  and  $D(s)$  are given,  $(u, v)$  are determined by  $\boldsymbol{\beta}$ . For fixed  $\mathbf{y}(s)$ ,  $D(s)$  is constant, and equispacial cone-beam projection data are denoted as  $g(s, u, v)$  with

$$u = \frac{D(s)\boldsymbol{\beta} \cdot \mathbf{d}_1}{\boldsymbol{\beta} \cdot \mathbf{d}_3}, \quad v = \frac{D(s)\boldsymbol{\beta} \cdot \mathbf{d}_2}{\boldsymbol{\beta} \cdot \mathbf{d}_3}. \quad (3)$$

### 3. ALGORITHMS

The proposed Katsevich-type algorithms with nonstandard spiral loci can be implemented in either the FBP or BPF format. Given the page limitation, we will describe them in the following subsections without some mathematical details/proofs.

#### 3.1 FILTERED BACKPROJECTION

The generic Katsevich algorithm was formulated in the FBP format, and can be generalized for nonstandard spiral cone-beam CT. Such a generalized algorithm consists of the following four steps.

##### Step 1: Cone-Beam Data Differentiation.

Keeping  $\boldsymbol{\beta}$  intact and using the chain rule, the derivative of cone-beam data with respect to  $s$  can be written as

$$\begin{aligned} G(s, u, v) &\equiv \frac{d}{ds} g(s, u, v) |_{\boldsymbol{\beta} \text{ fixed}} \\ &= \left( \frac{\partial}{\partial s} + \frac{R'(s)u + u^2 + D^2(s)}{D(s)} \frac{\partial}{\partial u} + \frac{R'(s)v + uv}{D(s)} \frac{\partial}{\partial v} \right) g(s, u, v) \end{aligned} \quad (4)$$

To compute the derivatives, a finite difference formula can be used.

##### Step 2: PI-Line Determination.

Assume the nonstandard spiral locus satisfies our conditions for existence and uniqueness of the PI-line, the following procedure can be used to determine the PI segment  $I_{PI(\mathbf{x})}$  for any given point  $\mathbf{x} \in \mathbf{U}$ . Let the two ends of the PI segment  $I_{PI(\mathbf{x})}$  be  $s_b(\mathbf{x})$  and  $s_t(\mathbf{x})$ . Theoretically, there must be a unique triplet  $s_b$ ,  $s_t$  and  $t$  with  $t \in (0, 1)$  and  $0 < s_t - s_b < 2\pi$  such that  $\mathbf{x} = t\mathbf{y}(s_b) + (1-t)\mathbf{y}(s_t)$ . First, we consider a family of the

PI-lines intersecting the vertical line  $V$  containing  $\mathbf{x}$ . This family of PI-lines can be parameterized by  $s_b$ . Through a fixed  $\mathbf{y}(s_b)$ , we can numerically find the PI-line that intersects the line  $V$  and  $\mathbf{y}(s_t)$  with  $s_t \in (s_b, s_b + 2\pi)$ . Because the longitudinal coordinate of such an interaction is an increasing function of  $s_b$ , using dichotomy we can numerically identify the unique  $s_b$  and  $s_t$  so that  $I_{PI(\mathbf{x})}$  contains  $\mathbf{x} \in \mathbf{U}$ .

**Step 3: Slant filtration.**

The generic Katsevich algorithm requires a slant filtering on the detector plane. In the standard helical scanning case, the involved filtering lines are independent of the source position. However, in the nonstandard spiral scanning case, the filtering paths depend on the source, detector and object locations. Following the same derivative as Appendix B in Reference [15], we get equation for filtering paths

$$v = \frac{h\Delta}{2\pi} \frac{D(s)[R(s_2)\sin(2\Delta) - 2R(s_1)\sin(\Delta)] + [R(s) - 2R(s_1)\cos(\Delta) + R(s_2)\cos(2\Delta)]u}{R(s)R(s_2)\sin(2\Delta) - R(s_1)\sin(\Delta)[R(s) + R(s_2)]}, \quad (5)$$

where the relations  $s_1 = \frac{s + s_2}{2}$  and  $\Delta = s_1 - s$  are used. If  $s_2 = s$ , (5) becomes

$$v = \frac{h}{2\pi} \frac{-2D(s)R'(s) + (R(s) - R''(s))u}{(R(s))^2 + 2(R'(s))^2 - R(s)R''(s)} \quad s = s_1 = s_2 \quad (6)$$

It can be proved that the proposed Katsevich-type formula with the nonstandard spiral locus allows exact reconstruction from truncated cone-beam data as defined by the extended Tam-Danielson window.

**Step 4: Weighted Backprojection.**

The filtered data at different source positions within the PI interval contribute to the reconstruction at  $\mathbf{x}$  according to weight inversely proportional to the distance from  $\mathbf{x}$  to the source  $\mathbf{y}(s)$ . This step is essentially the same as the 3D backprojection used in the Feldkamp-type reconstruction. It must be pointed out that the detector area required in the Katsevich-type reconstruction is larger than the extended Tam-Danielsson window depicted by the projected upper and lower spiral half turns.

**3.2 BACKPROJECTION FILTRATION**

Recently, Zou and Pan reformulated the generic Katsevich algorithm for backprojected filtration in the standard helical cone-beam geometry<sup>16</sup>. Similar to what Zou and Pan did, we constructed the following modified backprojected filtration (BPF) algorithm for variable radius spiral cone-beam CT/micro-CT.

**Step 1: Derivative Cone-Beam Data.**

The operations are the same as in the preceding subsection.

**Step 2: PI-Line Determination.**

The operations are the same as in the above subsection.

**Step 3: Weighted Backprojection.**

We can calculate the weighted 3D backprojection  $p(\mathbf{x}')$  of the cone-beam data derivatives onto a fixed PI-line segment  $I_{PI(\mathbf{x})}$ :

$$p(\mathbf{x}') = \int_{s_l(\mathbf{x})}^{s_b(\mathbf{x})} \frac{G(s, \tilde{u}, \tilde{v})}{|\mathbf{x}' - \mathbf{y}(s)|} ds \quad (7)$$

with

$$\tilde{u} = \frac{D(s)(\mathbf{x}' - \mathbf{y}(s)) \cdot \mathbf{d}_1}{(\mathbf{x}' - \mathbf{y}(s)) \cdot \mathbf{d}_3}, \tilde{v} = \frac{D(s)(\mathbf{x}' - \mathbf{y}(s)) \cdot \mathbf{d}_2}{(\mathbf{x}' - \mathbf{y}(s)) \cdot \mathbf{d}_3} \quad (8)$$

In fact, we only need calculate the values of  $p(\mathbf{x}')$  at discrete sampling points. Hence, we may denote the value of  $p(\mathbf{x}')$  as  $p(\tilde{x}_l)$ , where  $l = 0, 1, \dots, L-1, L$  indexing the data along the axis  $\tilde{x}$  that is coincident with the PI-line.

#### Step 4: Inverse Hilbert Transform.

According to the formulation by Zou and Pan<sup>16</sup>, we have

$$p(\tilde{x}) = 2 \int_{\tilde{x}_b}^{\tilde{x}_l} \frac{f(\tilde{x}')}{\tilde{x} - \tilde{x}'} d\tilde{x}' \quad (9)$$

where  $[\tilde{x}_b, \tilde{x}_l]$  covers the PI segment  $I_{PI(\mathbf{x})}$ . This relationship can be put in a matrix form linking  $p(\tilde{x}_l)$  and  $f(\tilde{x}_l)$  at the discrete sampling points along the axis  $\tilde{x}$ . Then, we can invert the system to obtain  $f(\tilde{x}_l)$ .

## 4. NUMERICAL SIMULATIONS

In our numerical simulation, two variable radius loci for evaluation and verification of the proposed algorithms were used, which are described by  $R(s) = R_a + R_b \cos(s)$  and  $R(s) = R_a + \frac{R_b}{2\pi} s$ . For convenience, we will refer them as NVRL (nonlinear variable radius locus) and LVRL (linear variable radius locus), respectively. We set  $R_a = 87.5\text{cm}$  and  $R_b = 12.5\text{cm}$  for NVRL, while  $R_a = 90.0\text{cm}$  and  $R_b = 30.0\text{cm}$  for LVRL. In the following, unless otherwise stated others parameters should remain the same as in Table 1.

Table 1 Cone-beam imaging parameters used in the numerical simulation

Origin to detector distance ( $D_c$ )	75cm
Helical pitch (h)	12.5cm
Object radius (r)	25cm
Scanning range	$s \in [-2\pi, 2\pi]$
Scanning angle sampling interval ( $\Delta s$ )	$\pi/400$
Horizontal detector sampling interval ( $\Delta u$ )	0.333cm
Vertical detector sampling interval ( $\Delta v$ )	0.333cm
Reconstruction matrix	$256 \times 256 \times 256$

The modified 3D Shepp-Logan phantom was used, which includes 10 ellipsoids with normalized parameters as listed in Table 2, where  $(x_0, y_0, z_0)$  are the coordinates of an ellipsoid center,  $(a, b, c)$  the  $x, y, z$  semi-axes,  $\phi$  is the rotation angle of an ellipsoid (about  $z$  axis), and  $f$  is the relative X-ray linear absorption coefficient. The effective X-ray absorption coefficient of a point is the sum of the relative parameters of those ellipsoids that contain the point.

Following the same numerical implementation steps as that of the FBP algorithm for standard spiral cone beam CT<sup>15,19</sup>, we implemented the FBP algorithm described in Subsection 3.1 for variable radius spiral cone-beam CT in MatLab and C. Fig. 2 shows some reconstructed slices by the Katsevich-type FBP algorithm. The first row presents slices reconstructed from cone-beam projections collected from NVRL, while the second row is for the counterparts from LVRL. The left column includes slices at  $z=-6.25\text{cm}$ , the middle column at  $y=0\text{cm}$ , and right column at  $x=0\text{cm}$ . The gray-level interval  $[0.1, 0.3]$  was mapped  $[0, 255]$  for visualization. As shown in Fig.2, it can be seen that the FBP algorithm worked well for both NVRL and LVRL.

Table 2. Normalized parameters of the modified 3D Shepp-Logan phantom

No.	$a$	$b$	$c$	$x_0$	$y_0$	$z_0$	$\phi$	$f$
1	0.6900	0.920	0.900	0	0	0	0	1.0
2	0.6624	0.874	0.880	0	0	0	0	-0.8
3	0.4100	0.160	0.210	-0.22	0	-0.250	108	-0.2
4	0.3100	0.110	0.220	0.22	0	-0.25	72	-0.2
5	0.2100	0.250	0.500	0	0.35	-0.25	0	0.2
6	0.0460	0.046	0.046	0	0.1	-0.25	0	0.2
7	0.0460	0.023	0.020	-0.08	-0.65	-0.25	0	0.1
8	0.0460	0.023	0.020	0.06	-0.65	-0.25	90	0.1
9	0.0560	0.040	0.100	0.06	-0.105	0.625	90	0.2
10	0.0560	0.056	0.100	0	0.100	0.625	0	-0.2

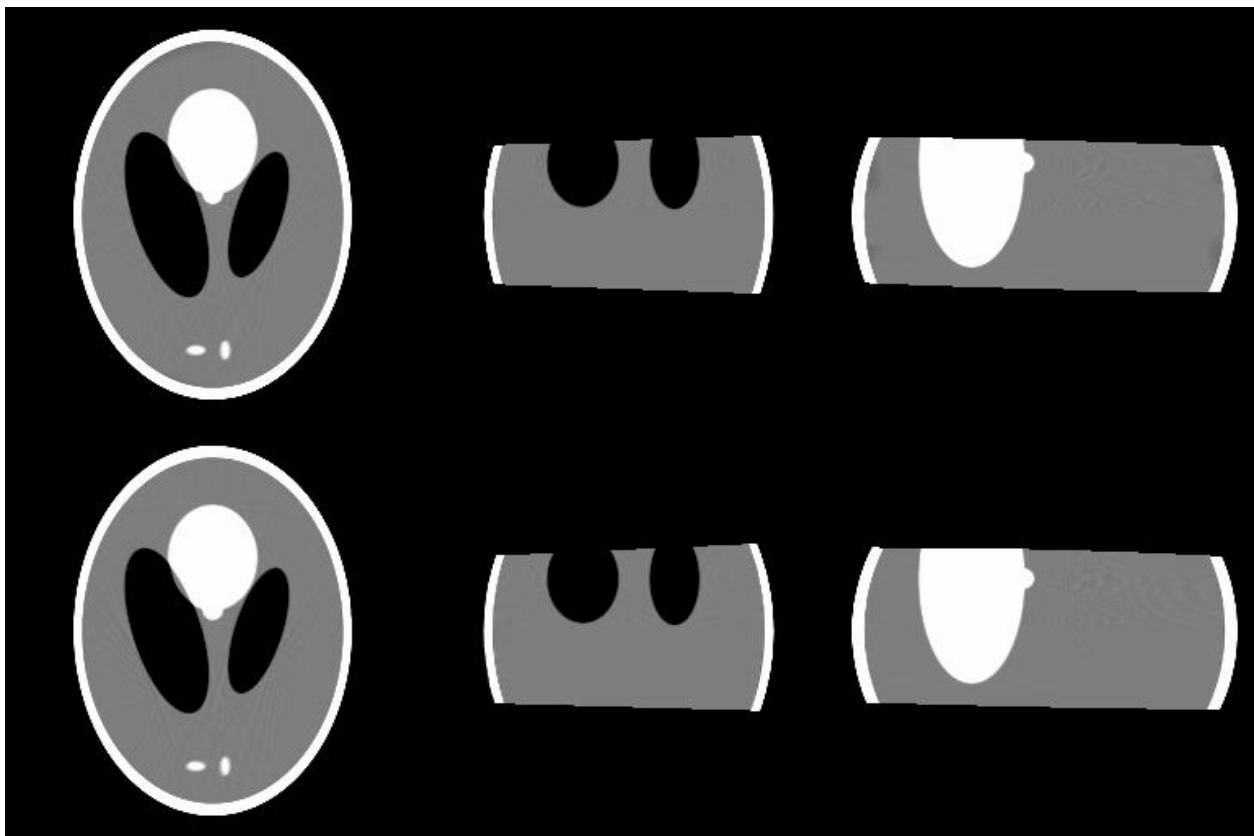


Figure 2. Reconstructed slices of the modified 3D Shepp-Logan Phantom by our Katsevich-type FBP algorithm

Also, we implemented the BPF algorithm described in Subsection 3.2 for variable radius spiral cone-beam CT in MatLab. Then, we reconstructed the modified 3D Shepp-Logan phantom on PI-lines specified by a fixed  $s_b$  and a set of  $s_t$ . Fig. 3 shows representative reconstruction results. The first row gives slices reconstructed from cone-beam projections collected from NVRL, while the second row is for LVRL. The PI-lines for the left column are  $s_b = -\pi$  and  $s_t \in [-0.32\pi, 0.32\pi]$ , the PI-lines for the middle column  $s_b = -0.5\pi$  and  $s_t \in [0.18\pi, 0.82\pi]$ , and the PI-lines for the right column  $s_b = 0$  and  $s_t \in [0.68\pi, 1.32\pi]$ . The gray-level range was windowed in the same way as above. These slices appear somewhat “distorted” because they are not displayed in the Cartesian coordinate system, but for any given point  $\mathbf{x}$ , the reconstruction value can be readily obtained with 3D interpolation.

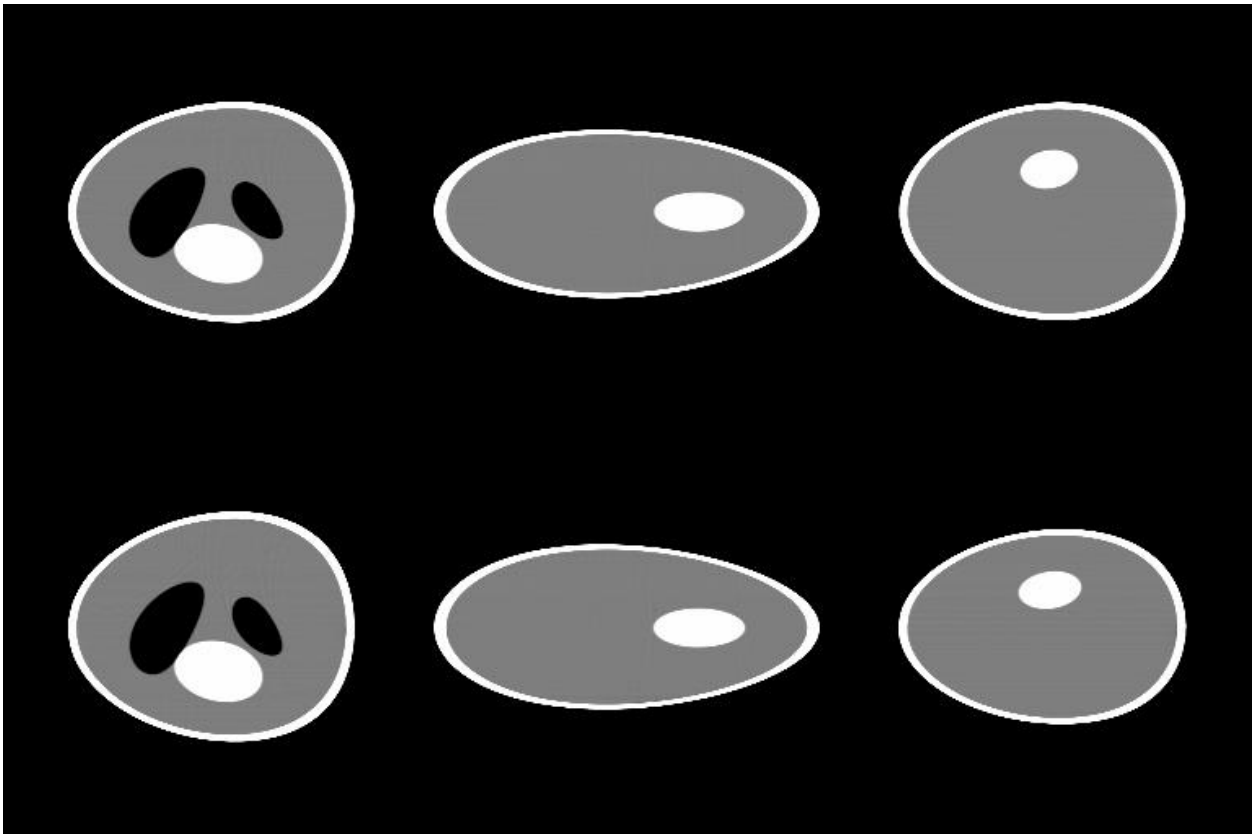


Figure 3. Reconstructed slices of the modified 3D Sheep-Logan Phantom by our Katsevich-type BPF algorithm

## 5. CONCLUSION

In conclusion we have proposed two Katsevich-type reconstruction algorithms in case of variable radius spiral cone-beam scanning. The Katsevich-type FBP algorithm needs more projection data while the Katsevich-type BPF algorithm only uses the data in the extended Tam-Danielsson window. However, the Katsevich-type FBP algorithm seems producing better image quality than the Katsevich-type BPF algorithm. We will report related theoretical results and more comparative data in other publications.

## ACKNOWLEDGEMENTS

This work is partially supported by a Carver Scientific Research Initiative grant and NIH/NIBIB grants EB002667 and EB004287.

## REFERENCES

1. G. Wang, TH Lin, PC Cheng, DM Shinozaki, HG Kim; Scanning cone-beam reconstruction algorithms for x-ray microtomography; *Proc. SPIE Vol. 1556*, p. 99-112, July 1991.
2. X. H. Yan and R. M. Leahy; Cone beam tomography with circular, elliptical and spiral orbits; *Physics in Medicine and Biology*, vol. 37, pp. 493–506, 1992.
3. H. Kudo, F. Noo, M. Defrise; Cone-beam filtered-backprojection algorithm for truncated data; *Physics in Medicine and Biology*, vol 43:2885-2909, 1998.
4. K. C. Tam, S. Samarasekera, and F. Sauer; Exact cone-beam CT with a spiral scan; *Physics in Medicine and Biology*, vol. 43, pp. 1015–1024, 1998.
5. G. Wang, G. D. Schweiger, and M. W. Vannier; An iterative algorithm for X-ray CT fluoroscopy, *IEEE Trans. Medical Imaging.*, vol. 17, pp. 853–856, 1998.
6. S. Zhao and G. Wang; Feldkamp-type cone-beam tomography in the wavelet framework; *IEEE Trans. Med. Imag.*; 19(9): 922–929, 2000.
7. M. Defrise, F. Noo, and H. Kudo; Quasi-exact filtered backprojection algorithm for long-object problem in helical cone-beam tomography; *IEEE Trans. Med. Imag.*, 19(9). 902–921, 2000
8. M. Defrise, F. Noo, and H. Kudo; A solution to the long-object problem in helical cone-beam tomography; *Physics in Medicine and Biology*, vol. 45, pp. 623–643, 2000.
9. G. Wang, C.R. Crawford, W.A. Kalender, “Multi-row-detector and cone-beam spiral/helical CT”, *IEEE Trans. Med. Imaging* 19(9):817-821, 2000.
10. A. Katsevich; “Theoretically exact fbp-type inversion algorithm for spiral CT,” *SIAM J. Appl.Math*, vol. 62, pp. 2012-2026, 2002.
11. A. Katsevich, “Improved exact FBP algorithm for spiral CT”, *Adv. Appl. Math*, 32:681-697, 2004.
12. A. Katsevich, “Analysis of an exact inversion algorithm for spiral cone-beam CT”. *Physics in Medicine and Biology*. 47: 2583-2597, 2002.
13. A. Katsevich., et al. “Evaluation and empirical analysis of an exact FBP algorithm for spiral cone-beam CT”, *Proceedings of SPIE Vol 5032 II: 663-674, 2003*, San Diego.
14. F. Noo, J. Pack, and D. Heuscher, “Exact helical reconstruction using native cone-beam geometries”, *Physics in Medicine and Biology.*, 48:3787-3818, 2003.
15. H. Yu and G. Wang, “Studies on Implementation of the Katsevich Algorithm for Spiral Cone-beam CT”, *Journal of X-ray Science and Technology*; 12(2), 2004.
16. Y. Zou and X. Pan, “Exact image reconstruction on PI-lines in helical cone beam CT,” *Physics in Medicine and Biology*. 49: 941-959, 2004.
17. Y. Ye, J. Zhu and G. Wang, “Minimum Detection Windows, PI-Line Existence, and Uniqueness for Helical Cone-Beam Scanning of Variable Pitch”, *Medical Physics*; 31(3):566-572, 2004.
18. Y. Ye, J. Zhu and G. Wang, “Geometric Studies on Variable Radius Spiral Cone Beam Scanning,” *Medical Physics*, 31(6):1473-1480, 2004.
19. H. Yu, and G. Wang, “Studies on artifacts of the Katsevich algorithm for spiral cone-beam CT”, *Proceedings of SPIE*, Vol 5535, August 2004.
20. Y. Ye and G. Wang, “Cone beam reconstruction along a 3D spiral of a variable radius and/or variable pitch”, *Proceedings of SPIE*, Vol 5535, August 2004.
21. S. Zhao, H. Yu and G. Wang, “A family of Katsevich-type FBP algorithms for spiral cone-beam CT”, *Proceedings of SPIE*, Vol 5535, August 2004.
22. G. Wang and Y. Ye, “Nontrivial spiral cone-beam scanning methods, apparatus, and applications,” Patent disclosure filled with University of Iowa, November 2003, (US provisional patent application pending).